

Constraining extended scalar sectors at current and future colliders

Tania Robens^{a,b,*}

^a*Division of Theoretical Physics, Rudjer Boskovic Institute
Bijenicka cesta 54, 10000 Zagreb, Croatia*

^b*Theoretical Physics Department, CERN
1211 Geneva 23, Switzerland*

E-mail: trobens@irb.hr

In this proceeding, I summarize results on various new physics extensions of the Standard Model, for models with and without dark matter candidates. I discuss current constraints as well as rates and discovery prospects at future colliders.

RBI-ThPhys-2022-12, CERN-TH-2022-056

*Corfu Summer Institute 2021 "School and Workshops on Elementary Particle Physics and Gravity"
29 August - 9 October 2021
Corfu, Greece*

*Speaker

1. Introduction

In this proceeding, I discuss various new physics models that extend the Standard Model (SM) by adding additional fields that transform as either singlets or doublets under the standard model gauge group. Most of the results presented here have already been discussed elsewhere, and I summarize our previous findings here. In particular, I discuss

- The real singlet extension of the SM, which comes with an additional scalar that transforms as a singlet. The model features one additional CP even neutral scalar. See [1–5] for original literature as well as [6] for results presented here;
- The Inert Doublet Model (IDM) [7–9], a two Higgs doublet model (THDM) with an additional \mathbb{Z}_2 symmetry that provides a dark matter (DM) candidate. Our original work can be found in [4, 10–12];
- The two real singlet extension (TRSM), where the SM scalar sector is extended by two additional gauge singlets, featuring in total three CP even neutral scalars that also allow for interesting cascade decays. The results discussed here have first been presented in [13, 14];
- The THDMa, a two higgs doublet model that is enhanced by an additional pseudoscalar which serves as a portal to the dark matter sector. In the version of the model discussed here, the DM candidate is fermionic. See [15–21] for original work and [22] for work containing the results discussed here.

All models are confronted with most recent theoretical and experimental constraints. Theory constraints include the minimization of the vacuum as well as the requirement of vacuum stability and positivity. We also apply constraints from perturbative unitarity and perturbativity of the couplings at the electroweak scale.

Experimental bounds include the agreement with current measurements of the properties of the 125 GeV resonance discovered by the LHC experiments, as well as agreement with the null-results from searches for additional particles at current or past colliders. Furthermore, we impose constraints from electroweak precision observables (via S , T , U parameters [23–25]), B-physics observables ($B \rightarrow X_s \gamma$, $B_s \rightarrow \mu^+ \mu^-$, ΔM_s), and astrophysical observables (relic density and direct detection bounds). We use a combination of private and public tools in these analyses. In particular, we use HiggsBounds [26], HiggsSignals [27], 2HDMC [28], SPheno [29], Sarah [30], micrOMEGAs [31, 32], and MadDM [33]. Experimental numbers are taken from [34, 35] for electroweak precision observables, [36] for $B_s \rightarrow \mu^+ \mu^-$, [37] for ΔM_s and [38] and [39] for relic density and direct detection, respectively. Bounds from $B \rightarrow X_s \gamma$ are implemented via a fit function from [40, 41]. Predictions for production cross sections shown here have been obtained using Madgraph5 [42].

2. Real singlet extension

As a first simple example, we discuss a real singlet extension of the SM with a \mathbb{Z}_2 symmetry previously reported on in [1–5, 43]. The \mathbb{Z}_2 symmetry is softly broken by a vacuum expectation

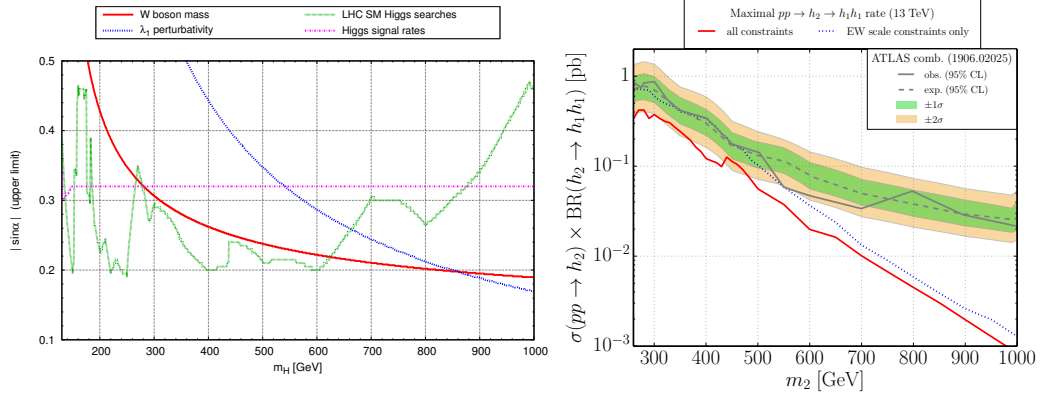


Figure 1: Results for the singlet extension, taken from [6]. *Left:* comparison of current constraints for a fixed value of $\tan\beta = 0.1$. *Right:* maximal $H \rightarrow hh$ allowed, with electroweak constraints at the electroweak scale (blue) or including RGE running to a higher scale (red), in comparison with results from the ATLAS combination.

value (vev) of the singlet field, inducing mixing between the gauge-eigenstates which introduces a mixing angle α . The model has in total 5 free parameters. Two of these are fixed by the measurement of the 125 GeV resonance mass and electroweak precision observables. We then have

$$\sin\alpha, m_2, \tan\beta \equiv \frac{v}{v_s} \quad (1)$$

as free parameters of the model, where v (v_s) are the doublet and singlet vevs, respectively. We concentrate on the case where $m_2 \geq 125$ GeV, where SM decoupling corresponds to $\sin\alpha \rightarrow 0$.

Limits on this model are shown in figure 1, taken from [6]¹, including a comparison of the currently maximal available rate of $H \rightarrow h_{125}h_{125}$ with the combination limits from ATLAS [44]. The most constraining direct search bounds are in general dominated by searches for diboson final states [45–48]. In some regions, the Run 1 Higgs combination [49] is also important. Especially [47, 48] currently correspond to the best probes of the models parameter space².

3. Inert Doublet Model

The Inert Doublet Model is a two Higgs doublet model with an exact discrete \mathbb{Z}_2 symmetry. It provides a dark matter candidate that stems from the second doublet [7–9]. The particle content of the model consists of four additional scalar states H , A , H^\pm , and has in total 7 free parameters prior to electroweak symmetry breaking:

$$v, m_h, \underbrace{m_H, m_A, m_{H^\pm}}_{\text{second doublet}}, \lambda_2, \lambda_{345} \equiv \lambda_3 + \lambda_4 + \lambda_5, \quad (2)$$

Here, the λ_i s denote standard couplings appearing in the THDM potential. Two parameters (m_h and v) are fixed by current measurements. The model has been subjected to various experimental

¹Updates will be presented in the proceedings of Moriond2022.

²We include searches currently available via HiggsBounds.

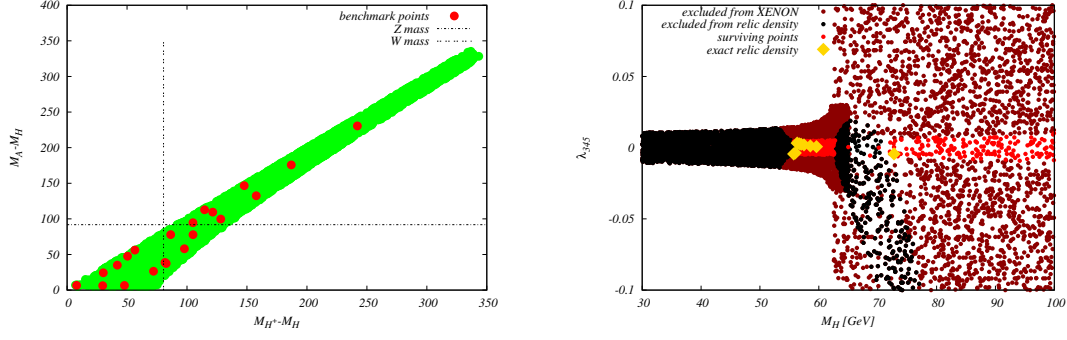


Figure 2: *Left:* Masses are requested to be quite degenerate after all constraints have been taken into account. In the $(M_{H^\pm} - M_H, M_A - M_H)$ plane (taken from [11]). *Right:* Interplay of signal strength and relic density constraints in the (M_H, λ_{345}) plane, using XENON1T results, with golden points labelling those points that produce exact relic density (taken from [4]).

collider	all others	AA	AA +VBF
HL-LHC	1 TeV	200-600 GeV	500-600 GeV
HE-LHC	2 TeV	400-1400 GeV	800-1400 GeV
FCC-hh	2 TeV	600-2000 GeV	1600-2000 GeV
CLIC, 3 TeV	2 TeV	-	300-600 GeV
$\mu\mu$, 10 TeV	2 TeV	-	400-1400 GeV
$\mu\mu$, 30 TeV	2 TeV	-	1800-2000 GeV

Table 1: Sensitivity of different collider options, using the sensitivity criterium of 1000 generated events in the specific channel. $x - y$ denotes minimal/ maximal mass scales that are reachable.

and theoretical constraints [4, 10–12, 50]. One important observation is the existence of a relatively strong degeneracy between the additional masses of the second doublet, as well as a minimal mass scale for the dark matter candidate H resulting from a combination of relic density and signal strength measurement constraints (see [10, 12] for a detailed discussion). We display these features in figure 2.

3.1 Sensitivity study at current and future colliders

I here present results first discussed in [12]. In that work, a sensitivity comparison for selected benchmark points [11, 12, 51] was used, which relies on a simple counting criteria: a benchmark point is considered reachable if at least 1000 signal events are produced using nominal luminosity of the respective collider (c.f. also [52]). Table 1 shows the results using this simple criterium. The accompanying figures, displaying production cross sections for pair-production of the novel scalars at various collider options and center-of-mass energies are shown in figure 3, taken from [12]. We here have used Madgraph5 [42] with a UFO input file from [53] for cross-section predictions. Results for CLIC were taken from [51, 54].

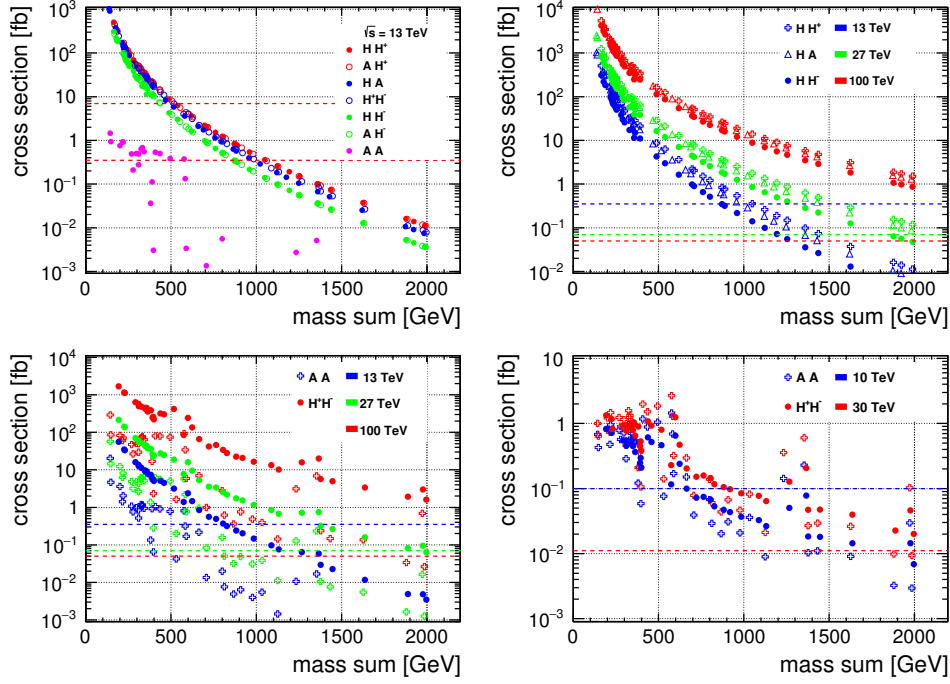


Figure 3: Predictions for production cross sections for various processes and collider options. *Top left:* Predictions for various pair-production cross sections for a pp collider at 13 TeV, as a function of the mass sum of the produced particles. *Top right:* Same for various center-of-mass energies. *Bottom left:* VBF-type production of AA and H^+H^- at various center-of-mass energies for pp colliders. *Bottom right:* Same for $\mu^+\mu^-$ colliders. Taken from [12]. The lines correspond to the cross-sections required to produce at least 1000 events using the respective design luminosity.

4. TRSM

In the TRSM [13], the SM scalar sector is augmented by two real scalars obeying a discrete $\mathbb{Z}_2 \otimes \mathbb{Z}'_2$ symmetry. Both fields acquire a vev, which induces a mixing between all scalar states. The model then has 9 a priori parameters after electroweak symmetry breaking,

$$m_1, m_2, m_3, v, v_X, v_S, \theta_{hS}, \theta_{hX}, \theta_{SX},$$

where m_i, v, θ denote masses³, vevs, and mixing angles. One mass $m \sim 125$ GeV and $v \sim 246$ GeV are fixed by current measurements.

Various benchmark planes (BPs) were proposed within this model [13], allowing for novel production and decay processes, including decay chains which by that time had not been investigated by the LHC experiments. Production and decay modes can be characterized as

$$p p \rightarrow h_3 \rightarrow h_1 h_2, p p \rightarrow h_a \rightarrow h_b h_b,$$

where for the symmetric decays we assume none of the scalars corresponds to the SM-like 125 GeV resonance.

³We use the convention $m_1 \leq m_2 \leq m_3$.

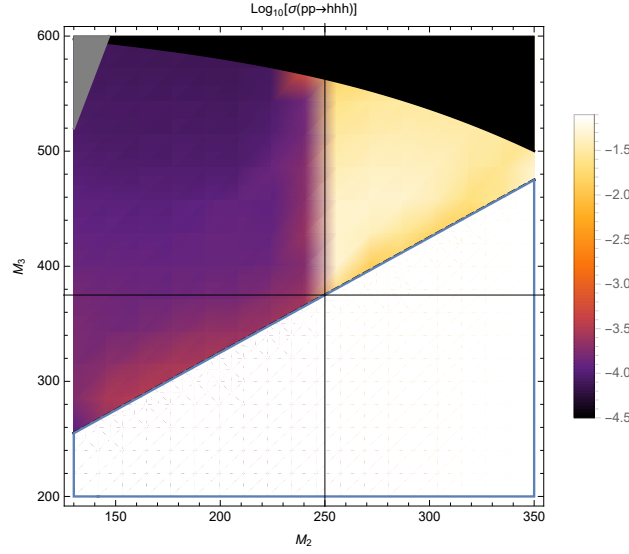


Figure 4: Production cross sections for $h_1 h_1 h_1$ production in BP3 at leading order, taken from [14]. See text for more details.

In [14], we focussed on one particular benchmark plane (BP3), that features the first production mode, in the scenario with $h_1 \equiv h_{125}$. This allows for a $h_{125} h_{125} h_{125}$ final state; production cross sections depend on the masses of the two additional scalars and are displayed in figure 4. We investigated the scenario where all h_{125} further decay into $b \bar{b}$ final states and conducted a complete phenomenological study for a 14 TeV LHC. We made use of a customized `loop_sm` model implemented in `MadGraph5_aMC@NLO` (v2.7.3) [55, 56], that was interfaced to `HERWIG` (v7.2.1) [57–63]. We have applied a semi-automated cut prescription to suppress SM background. Results are shown in table 2. We see that several benchmark points are already accessible with a relatively low integrated luminosity.

We refer the reader to the above work for details of the analysis as well as SM background simulation. Several of the benchmark points are in the $4\text{--}5\sigma$ range already for a relatively low luminosity, and all have significances above the discovery reach after the full run of HL-LHC.

Finally, we can ask whether other channels can not equally constrain the allowed parameter space at the HL-LHC. We therefore extrapolated various analyses assessing the heavy Higgs boson prospects of the HL-LHC in final states originating from $h_i \rightarrow h_1 h_1$ [44, 64], $h_i \rightarrow ZZ$ [47, 65] and $h_i \rightarrow W^+ W^-$ [66, 67], for $i = 2, 3$, and combined these with extrapolations of results from 13 TeV where appropriate. We display the results in figure 5.

In particular ZZ final states can probe nearly all of the available parameter space. These however depend on different model parameters than the $h_1 h_1 h_1$ final state rates. These searches are testing a different part of the parameter space and new physics potential.

(M_2, M_3) [GeV]	$\sigma(pp \rightarrow h_1 h_1 h_1)$ [fb]	$\sigma(pp \rightarrow 3b\bar{b})$ [fb]	$\text{sig} _{300\text{fb}^{-1}}$	$\text{sig} _{3000\text{fb}^{-1}}$
(255, 504)	32.40	6.40	2.92	9.23
(263, 455)	50.36	9.95	4.78	15.11
(287, 502)	39.61	7.82	4.01	12.68
(290, 454)	49.00	9.68	5.02	15.86
(320, 503)	35.88	7.09	3.76	11.88
(264, 504)	37.67	7.44	3.56	11.27
(280, 455)	51.00	10.07	5.18	16.39
(300, 475)	43.92	8.68	4.64	14.68
(310, 500)	37.90	7.49	4.09	12.94
(280, 500)	40.26	7.95	4.00	12.65

Table 2: 6 b final state leading-order production cross sections at 14 TeV, as well as significances for different integrated luminosities. Taken from [14].

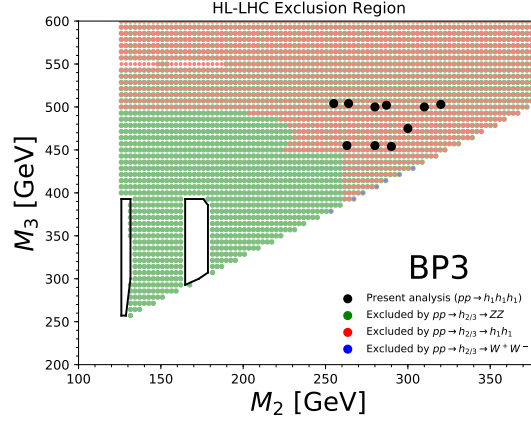


Figure 5: Constraints on the (M_2, M_3) plane from extrapolation of other searches at the HL-LHC from extrapolation (see text for details). Taken from [14].

5. THDMa

The THDMa has been widely promoted within the LHC Dark matter working group. It is a type II two-Higgs-doublet model that is extended by an additional pseudoscalar a mixing with the "standard" pseudoscalar A of the THDM. In the gauge-eigenbasis, the additional scalar serves as a portal to the dark sector, with a fermionic dark matter candidate, denoted by χ . More details can e.g. be found in [15–21].

The following mass eigenstates are incorporated within this model in the scalar and dark matter sector: h, H, H^\pm, a, A, χ . It depends on 12 additional new physics parameters

$$v, m_h, m_H, m_a, m_A, m_{H^\pm}, m_\chi; \cos(\beta - \alpha), \tan\beta, \sin\theta; y_\chi, \lambda_3, \lambda_{P_1}, \lambda_{P_2},$$

where v and either m_h or m_H are fixed by current measurements in the electroweak sector.

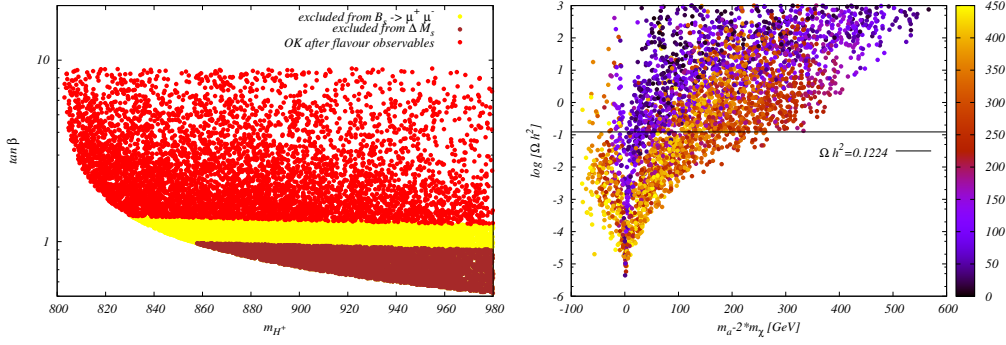


Figure 6: *Left:* Bounds on the $(m_{H^\pm}, \tan \beta)$ plane from B-physics observables, implemented via the SPheno [29]/ Sarah [30] interface, and compared to experimental bounds [36, 37]. The contour for low $(m_{H^\pm}, \tan \beta)$ values stems from [40, 41]. *Right:* Dark matter constraints in the THDMa model. *Right:* Dark matter relic density as a function of $m_a - 2m_\chi$, with m_χ defining the color coding. The typical resonance-enhanced relic density annihilation is clearly visible. Figures taken from [21].

In [21], a scan was presented that allows all of the above novel parameters float in specific predefined ranges. It is then not always straightforward to display bounds from specific constraints in 2-dimensional planes. Two examples where this is possible are shown in figure 6. The first plot displays bounds in the $(m_{H^\pm}, \tan \beta)$ plane from B-physics observables, and shows that in general low masses $m_{H^\pm} \lesssim 800$ GeV as well as values $\tan \beta \lesssim 1$ are excluded. The second plot displays the relic density as a function of the mass difference $m_a - 2m_\chi$. In the region where this mass difference remains small, relic density annihilates sufficiently to stay below the observed relic density bound. On the other hand, too large differences lead to values $\Omega h_c \gtrsim 0.12$ and therefore are forbidden [38].

For these scans, it was investigated which cross-section values would still be feasible for points that fulfill all constraints [21] at e^+e^- colliders. A particular interest lies on signatures that include missing energy and therefore distinguish this model from signatures that would be realized in a THDM without a portal to the dark sector. Processes like $e^+e^- \rightarrow hA, ha$ are suppressed due to alignment, which makes $e^+e^- \rightarrow HA, Ha$ the most interesting channel that contains novel signatures. However, such parameter points typically have mass scales $\gtrsim 1$ TeV. In such a case, production cross sections for an e^+e^- collider with a center-of-mass energy of 3 TeV are of interest. The corresponding production cross sections are shown in figure 7, which displays predictions for $t\bar{t}t\bar{t}$ and $t\bar{t} + \cancel{E}$ final states using a factorized approach. There is a non-negligible number of points where the second channel is dominant. A "best" point with a large rate for $t\bar{t} + \cancel{E}_\perp$ has been presented in [21].

6. Summary and Conclusion

In this work, I have reported on some previously published results for models that extend the scalar sector of the SM by additional gauge singlets or doublets. Some of the models discussed here in addition feature a dark matter candidate. I have presented results of applying current

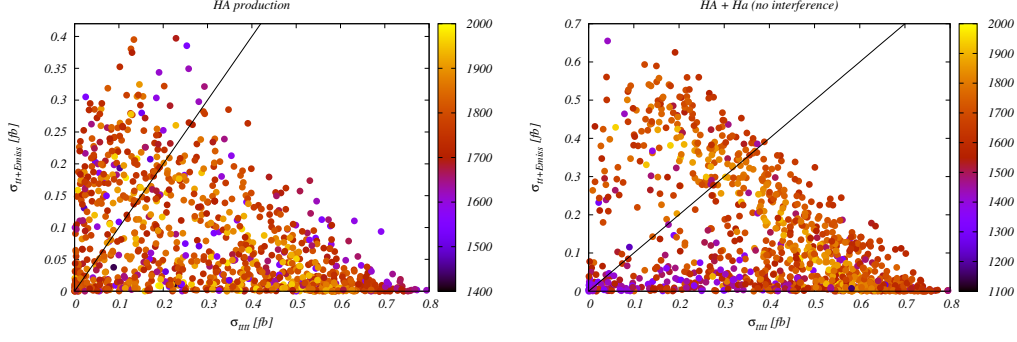


Figure 7: Production cross sections for $t\bar{t}t\bar{t}$ (x-axis) and $t\bar{t} + \cancel{E}$ (y-axis) final state in a factorized approach, for an e^+e^- collider with a 3 TeV center-of-mass energy. *Left:* mediated via HA , *right:* mediated via HA and Ha intermediate states. Color coding refers to $m_H + m_A$ (left) and $M_H + 0.5 \times (m_A + m_a)$ (right). Figures taken from [21].

constraints on these models, and rendered predictions for rates or significances at various future collider options. Some of the models presented here, in particular the IDM and TRSM, have not yet been fully explored by current collider experiments. I therefore strongly encourage the experimental collaborations to consider these at LHC Run III.

7. Acknowledgements

This research was supported in parts by the National Science Centre, Poland, the HARMONIA project under contract UMO-2015/18/M/ST2/00518 and OPUS project under contract UMO-2017/25/B/ST2/00496 (2018-2021), by the European Union through the Programme Horizon 2020 via the COST actions CA15108 - FUNDAMENTALCONNECTIONS and CA16201 - PARTICLEFACE, and by the UK's Royal Society.

References

- [1] G. M. Pruna and T. Robens, Phys. Rev. **D88**, 115012 (2013), 1303.1150.
- [2] T. Robens and T. Stefaniak, Eur. Phys. J. **C75**, 104 (2015), 1501.02234.
- [3] T. Robens and T. Stefaniak, Eur. Phys. J. **C76**, 268 (2016), 1601.07880.
- [4] A. Ilnicka, T. Robens, and T. Stefaniak, Mod. Phys. Lett. A **33**, 1830007 (2018), 1803.03594.
- [5] J. Alison *et al.*, (2019), 1910.00012, [Rev. Phys.5,100045(2020)].
- [6] T. Robens, Extended scalar sectors at current and future colliders, in *55th Rencontres de Moriond on QCD and High Energy Interactions*, 2021, 2105.07719.
- [7] N. G. Deshpande and E. Ma, Phys. Rev. **D18**, 2574 (1978).
- [8] Q.-H. Cao, E. Ma, and G. Rajasekaran, Phys. Rev. **D76**, 095011 (2007), 0708.2939.

- [9] R. Barbieri, L. J. Hall, and V. S. Rychkov, *Phys. Rev.* **D74**, 015007 (2006), hep-ph/0603188.
- [10] A. Ilnicka, M. Krawczyk, and T. Robens, *Phys. Rev. D* **93**, 055026 (2016), 1508.01671.
- [11] J. Kalinowski, W. Kotlarski, T. Robens, D. Sokolowska, and A. F. Zarnecki, *JHEP* **12**, 081 (2018), 1809.07712.
- [12] J. Kalinowski, T. Robens, D. Sokolowska, and A. F. Zarnecki, *Symmetry* **13**, 991 (2021), 2012.14818.
- [13] T. Robens, T. Stefaniak, and J. Wittbrodt, *Eur. Phys. J. C* **80**, 151 (2020), 1908.08554.
- [14] A. Papaefstathiou, T. Robens, and G. Tetlalmatzi-Xolocotzi, *JHEP* **05**, 193 (2021), 2101.00037.
- [15] S. Ipek, D. McKeen, and A. E. Nelson, *Phys. Rev.* **D90**, 055021 (2014), 1404.3716.
- [16] J. M. No, *Phys. Rev.* **D93**, 031701 (2016), 1509.01110.
- [17] D. Goncalves, P. A. N. Machado, and J. M. No, *Phys. Rev.* **D95**, 055027 (2017), 1611.04593.
- [18] M. Bauer, U. Haisch, and F. Kahlhoefer, *JHEP* **05**, 138 (2017), 1701.07427.
- [19] P. Tunney, J. M. No, and M. Fairbairn, *Phys. Rev.* **D96**, 095020 (2017), 1705.09670.
- [20] LHC Dark Matter Working Group, T. Abe *et al.*, *Phys. Dark Univ.* **27**, 100351 (2020), 1810.09420.
- [21] T. Robens, *Symmetry* **13**, 2341 (2021), 2106.02962.
- [22] J. Kalinowski, T. Robens, and A. F. Zarnecki, New Physics with missing energy at future lepton colliders - Snowmass White Paper, in *2022 Snowmass Summer Study, 2022*, 2203.07913.
- [23] G. Altarelli and R. Barbieri, *Phys. Lett.* **B253**, 161 (1991).
- [24] M. E. Peskin and T. Takeuchi, *Phys. Rev. Lett.* **65**, 964 (1990).
- [25] M. E. Peskin and T. Takeuchi, *Phys. Rev.* **D46**, 381 (1992).
- [26] P. Bechtle *et al.*, *Eur. Phys. J. C* **80**, 1211 (2020), 2006.06007.
- [27] P. Bechtle *et al.*, *Eur. Phys. J. C* **81**, 145 (2021), 2012.09197.
- [28] D. Eriksson, J. Rathsmann, and O. Stål, *Comput. Phys. Commun.* **181**, 189 (2010), 0902.0851.
- [29] W. Porod and F. Staub, *Comput. Phys. Commun.* **183**, 2458 (2012), 1104.1573.
- [30] F. Staub, *Comput. Phys. Commun.* **185**, 1773 (2014), 1309.7223.
- [31] G. Bélanger, F. Boudjema, A. Goudelis, A. Pukhov, and B. Zaldivar, *Comput. Phys. Commun.* **231**, 173 (2018), 1801.03509.

- [32] G. Belanger, A. Mjallal, and A. Pukhov, *Eur. Phys. J. C* **81**, 239 (2021), 2003.08621.
- [33] F. Ambrogio *et al.*, *Phys. Dark Univ.* **24**, 100249 (2019), 1804.00044.
- [34] Gfitter Group, M. Baak *et al.*, *Eur. Phys. J.* **C74**, 3046 (2014), 1407.3792.
- [35] J. Haller *et al.*, *Eur. Phys. J.* **C78**, 675 (2018), 1803.01853.
- [36] CMS-PAS-BPH-20-003, LHCb-CONF-2020-002, ATLAS-CONF-2020-049.
- [37] HFLAV, Y. S. Amhis *et al.*, *Eur. Phys. J.* **C81**, 226 (2021), 1909.12524.
- [38] Planck, N. Aghanim *et al.*, *Astron. Astrophys.* **641**, A6 (2020), 1807.06209, [Erratum: *Astron. Astrophys.* 652, C4 (2021)].
- [39] XENON, E. Aprile *et al.*, *Phys. Rev. Lett.* **121**, 111302 (2018), 1805.12562.
- [40] M. Misiak, A. Rehman, and M. Steinhauser, *JHEP* **06**, 175 (2020), 2002.01548.
- [41] M. Misiak, Private communication.
- [42] J. Alwall, M. Herquet, F. Maltoni, O. Mattelaer, and T. Stelzer, *JHEP* **06**, 128 (2011), 1106.0522.
- [43] LHC Higgs Cross Section Working Group, D. de Florian *et al.*, (2016), 1610.07922.
- [44] ATLAS, G. Aad *et al.*, *Phys. Lett.* **B800**, 135103 (2020), 1906.02025.
- [45] CERN Report No., , 2013 (unpublished), CMS-PAS-HIG-13-003.
- [46] CMS, V. Khachatryan *et al.*, *JHEP* **10**, 144 (2015), 1504.00936.
- [47] CMS, A. M. Sirunyan *et al.*, *JHEP* **06**, 127 (2018), 1804.01939, [Erratum: *JHEP*03,128(2019)].
- [48] ATLAS, M. Aaboud *et al.*, *Phys. Rev.* **D98**, 052008 (2018), 1808.02380.
- [49] CERN Report No., , 2012 (unpublished), CMS-PAS-HIG-12-045.
- [50] T. Robens, The IDM and THDMa – current constraints and future prospects, in *European Physical Society Conference on High Energy Physics 2021*, 2021, 2110.07294.
- [51] J. Kalinowski, W. Kotlarski, T. Robens, D. Sokolowska, and A. F. Zarnecki, *JHEP* **07**, 053 (2019), 1811.06952.
- [52] T. Robens, J. Kalinowski, A. F. Zarnecki, and A. Papaefstathiou, Extended scalar sectors at future colliders, in *27th Cracow Epiphany Conference on Future of particle physics*, 2021, 2104.00046.
- [53] A. Goudelis, B. Herrmann, and O. Stål, *JHEP* **09**, 106 (2013), 1303.3010.
- [54] J. de Blas *et al.*, **3/2018** (2018), 1812.02093.

- [55] J. Alwall *et al.*, JHEP **07**, 079 (2014), 1405.0301.
- [56] V. Hirschi and O. Mattelaer, JHEP **10**, 146 (2015), 1507.00020.
- [57] M. Bahr *et al.*, Eur. Phys. J. **C58**, 639 (2008), 0803.0883.
- [58] S. Gieseke *et al.*, (2011), 1102.1672.
- [59] K. Arnold *et al.*, (2012), 1205.4902.
- [60] J. Bellm *et al.*, (2013), 1310.6877.
- [61] J. Bellm *et al.*, Eur. Phys. J. **C76**, 196 (2016), 1512.01178.
- [62] J. Bellm *et al.*, (2017), 1705.06919.
- [63] J. Bellm *et al.*, Eur. Phys. J. **C80**, 452 (2020), 1912.06509.
- [64] CMS, A. M. Sirunyan *et al.*, Phys. Rev. Lett. **122**, 121803 (2019), 1811.09689.
- [65] M. Cepeda *et al.*, CERN Yellow Rep. Monogr. **7**, 221 (2019), 1902.00134.
- [66] ATLAS, M. Aaboud *et al.*, Eur. Phys. J. **C78**, 24 (2018), 1710.01123.
- [67] ATLAS, CERN Report No. ATL-PHYS-PUB-2018-022, 2018 (unpublished).